The crystal chemistry of synthetic potassium-bearing neighborite, (Na 1− x K x)MgF 3

Article *in* Physics and Chemistry of Minerals · May 2001

DOI: 10.1007/s002690100151

CITATIONS
28

READS
107

4 authors:

Anton Chakhmouradian
University of Manitoba
144 PUBLICATIONS **3,422** CITATIONS
SEE PROFILE

K. C. Ross
Laurentian University
9 PUBLICATIONS **114** CITATIONS
SEE PROFILE

Roger H. Mitchell
Lakehead University Thunder Bay Campus
327 PUBLICATIONS **9,689** CITATIONS
SEE PROFILE

Ian Swainson
International Atomic Energy Agency (IAEA)
211 PUBLICATIONS **4,462** CITATIONS
SEE PROFILE

Phys Chem Minerals (2001) 28: 277–284

ORIGINAL PAPER

A. R. Chakhmouradian · K. Ross
R. H. Mitchell · I. Swainson

The crystal chemistry of synthetic potassium-bearing neighborite, $(Na_{1-x}K_x)MgF_3$

Received: 10 May 2000 / Accepted: 6 November 2000

Abstract A series of fluoride perovskites related to neighborite was investigated using X-ray and neutron diffraction techniques, and Rietveld profile refinement of powder diffraction data. The series $(Na_{1-x}K_x)MgF_3$ comprises orthorhombic (*Pbnm*, $a \approx \sqrt{2}a_p$, $b \approx \sqrt{2}a_p$, $c \approx 2a_p$, $Z = 4$) perovskites in the compositional range $0 \le x \le 0.30$, tetragonal perovkites (*P4/mbm*, $a \approx \sqrt{2}a_p$, $c \approx a_p$, $Z = 2$) in the range $0.40 \le x \le 0.46$, and cubic phases ($Pm\bar{3}m$, $Z = 1$) for $x > 0.50$. The structure of the orthorhombic neighborite is derived from the perovskite aristotype by rotation of MgF_6 octahedra about the [110] and [001] axes of the cubic subcell. The degree of rotation, measured as a composite tilt Φ about the triad axis, varies from 18.2° at $x = 0$ to 11.2° at $x = 0.30$ (as determined from the fractional atomic coordinates). Orthorhombic neighborite also shows a significant displacement of Na and K from the "ideal" position (≤0.25 Å). The tetragonal members of the neighborite series exhibit only in-phase tilting about the [001] axis of the cubic subcell (ϕ) ranging from 4.5° to 4.8° (determined from the atomic coordinates). The solid solution $(Na_{1-x}K_x)MgF_3$, shows a regular variation of unit-cell dimensions with composition from 3.8347 Å for the end-member $NaMgF_3$ (reduced to pseudocubic subcell, a_p) to 3.9897 Å for $KMgF_3$. This variation is accompanied by increasing volumes of the *A*-site polyhedra, whereas the volume of MgF_6 octahedra initially decreases (up to $x = 0.40$), and then increases concomitantly with K content. The polyhedral volume ratio, V_A/V_B, gradually increases towards the tetragonal structural range, in agreement with diminishing octahedral rotation in the structure. The *P4/mbm*-type neighborite has an "anomalous" polyhedral volume ratio (ca. 5.04) owing to the critical compression of MgF_6 polyhedra.

Key words Perovskite · Neighborite · Crystal structure · Phase transition

A. R. Chakhmouradian (✉) · K. Ross · R. H. Mitchell
Department of Geology, Lakehead University,
955 Oliver Road, Thunder Bay,
Ontario P7B 5E1, Canada
Tel.: 1-807-343-8329; Fax: 1-807-346-7853
e-mail: achakhmo@gale.lakeheadu.ca

I. Swainson
Neutron Program for Materials Research,
Steacie Institute for Molecular Sciences,
National Research Laboratory, Chalk River,
Ontario K0J 1J0, Canada

Introduction

Crystal structures of perovskite-type compounds (ideally ABX_3) have been extensively studied over the past 50 years, as these phases have a number of potential and actual applications as ferroelectrics, ionic conductors, semiconductors, superconductors, magnetoresistors, fuel cells, and nuclear-waste repositories. The interest in these structures has been further stimulated by the hypothesis that the Mg-silicate perovskite is a major constituent of the Earth's lower mantle. Among perovskites (sensu lato), oxide compounds ($X = O$) incorporating a diversity of cations in the *A* and *B* sites, are structurally the best characterized. There is much less information available in the literature concerning fluoride perovskites ($A^{1+}B^{2+}F_3$) and, in particular, on miscibility between different fluoride end members and phase transitions associated with cationic substitutions in the *A* and *B* sites. To our knowledge, only the series $(K_xNa_{1-x})CaF_3$ (Mo et al. 1990), $K(Mg_{1-x}Cu_x)F_3$ (Burns et al. 1996), $(Na_{1-x}K_x)MgF_3$ (Zhao 1998), and $(Rb_{1-x}K_x)CaF_3$ (Flocken et al. 1996; Jouanneaux et al. 1998) have been structurally characterized in detail.

The mineral neighborite ($NaMgF_3$) was first described by Chao et al. (1961) in an oil shale of the Green River Formation, Utah. Subsequently, this mineral has been found in several other localities worldwide (Table 1). The petrographic and paragenetic diversity of neighborite occurrences suggests that this phase may be far more common in alkali-rich silicate rocks and

Table 1 Natural occurrences of neighborite: a summary

Locality	Rock type	Associated minerals	Reference
South Ouray[a] Utah, USA	Dolomitic oil shale (Green River Formation)	Burbankite, nahcolite, wurtzite, barytocalcite, garrelsite, pyrite, calcite, quartz	Chao et al. (1961)
Mont Saint-Hilaire Québec, Canada	Alkali pegmatite, hornfels in contact with nepheline syenite	Quartz, dolomite, rutile, brookite, calcite, epididymite, mckelvyite	Horváth and Gault (1990)
Lake Gjerdingen Norway	Alkali granite	Sellaite, gagarinite, gearksutite, thomsenolite, pachnolite, ralstonite, bastnäsite	Raade and Haug (1980)
Ural Mts., Russia	Alkali metasomatite	Albite, biotite, cancrinite, sodalite, analcime, fluorite, burbankite, calcite, ilmenite	Yefimov et al. (1967)
Eastern Siberia, Russia	Aegirine–amphibole and biotite–feldspar metasomatites	Quartz, feldspar, fluorite, gagarinite, monazite, weberite	Arkhangel'skaya (1974)
Khibina, Kola Peninsula, Russia	Calcite–carbonatite	Calcite, burbankite, ankerite, pyrrhotite, pyrite, galena, hydrotalcite (replacement product of neighborite)	Zaitsev (1992)
Oldoinyo Lengai[b] Tanzania	Alkali–carbonatite lava	Sodian sylvite, Ba–Ca–Sr carbonates, gregoryite, nyerereite	Mitchell (1997)

[a] Type locality
[b] Neighborite with high K contents

carbonatites than has been previously recognized. The potassium-dominant analogue of neighborite has been observed thus far only in a sample of carbonatitic lava from Oldoinyo Lengai, Tanzania (Mitchell 1997). This mineral shows a significant solid solution towards the $NaMgF_3$ end member (ca. 47 mol%). Unfortunately, the size of K–Na–Mg fluorides from Tanzania is too small (<10 μm) to allow their examination by conventional X-ray techniques. The present study was initiated to investigate the crystal chemistry of perovskite-type compounds in the series neighborite – "potassium neighborite", using synthetically prepared samples. When this work was approaching its completion, a structural investigation of the series $(Na_{1-x}K_x)MgF_3$ was published by Zhao (1998). As findings of this author are not in complete agreement with our data, a detailed comparison between the two sets of results is given below.

Synthesis and analytical techniques

The end members and intermediate perovskite compositions from the series $(Na_{1-x}K_x)MgF_3$ were prepared synthetically from stoichiometric amounts of NaF, KF, and MgF_2 (high purity grade) using the ceramic technique. The oven-dried reagents were ground in an agate mortar and heated first at 700–750 °C for 5–10 h and, after regrinding, at 750–800 °C for up to 12 h in alumina crucibles. The perovskite compositions were synthesized in air and in a nitrogen flow. Also, several intermediate compositions that proved to be the most structurally challenging ($0.30 \le x \le 0.50$), were resynthesized from stoichiometric amounts of the end-member fluorides $NaMgF_3$ and $KMgF_3$. These compositionally intermediate perovskites were prepared at 800 °C over time periods ranging from 10–12 h.

The synthesized samples were examined by conventional X-ray techniques using a Philips 3710 diffractometer operated at 30 mA and 40 kV. The X-ray diffraction (XRD) powder patterns (Ni-filtered Cu$K\alpha$ radiation) were recorded over the 2θ range from 10–140° in a step-scan mode with a step size of 0.02° and a counting time of 2 s per step. The samples of the two end-member fluorides ($x = 0$ and 1.00) and three intermediate compositions approaching inferred phase transitions ($x = 0.30$, 0.40, and 0.50) were also examined by neutron diffraction (ND) using the facility at Chalk River Laboratories (Atomic Energy Canada Limited, Ontario, Canada). The samples were packed into vanadium cylinders with a volume of approximately 1.5 cm^3, and examined using a DUALSPEC C2 high-resolution constant-wavelength powder diffractometer. For each sample, the wavelength was determined by profile refinement of an Al_2O_3 standard. A wavelength of 1.3302 Å was used for the end-member compounds, and wavelengths of 2.3700 and 2.3548 Å for the samples with $x = 0.30$ and $x = 0.40$–0.50, respectively. The neutron beam was monochromated using silicon. Reflections 531 and 311 were used to generate the low- and high-wavelength radiation, respectively, with a diffractometer takeoff angle of about 92.7°. The obtained XRD and ND patterns were further analyzed by the Rietveld (full-profile) refinement method using the FULLPROF software package (Rodriguez-Carvajal 1990). Diffraction lines were modeled using the pseudo-Voigt profile function, and the background was refined using a fifth-order polynomial.

Results

Complete solubility was observed between neighborite ($NaMgF_3$) and its potassium analogue $KMgF_3$. The XRD and ND patterns of all intermediate members of the solid solution $(Na_{1-x}K_x)MgF_3$ show predominantly diffraction peaks of perovskite-type phases. Minor diffraction lines indicative of MgF_2 and MgO are present in some XRD patterns, but their relative intensities do not

Table 2 $NaMgF_3$ ($x = 0$): comparison with previously published structural data

	This study		Zhao et al. (1993a)	Rönnebro et al. (2000)
	XRD[a]	ND[b]	XRD (Synchrotr.)	Single-crystal[c]
a (Å)	5.3607(1)	5.365(1)	5.3579(1)	5.3617(5)
b (Å)	5.4873(1)	5.492(1)	5.4842(1)	5.4897(3)
c (Å)	7.6662(1)	7.674(1)	7.6618(1)	7.6682(5)
Na				
x	0.9895(4)	0.9896(9)	0.9893(3)	0.9902(2)
y	0.0441(3)	0.0452(8)	0.0443(3)	0.0446(2)
z	¼	¼	¼	¼
B (Å^2)	1.89(4)	1.6(1)	1.71(5)	
Mg				
x	0	0	0	0
y	½	½	½	½
z	0	0	0	0
B (Å^2)	0.89(3)	0.42(9)	0.42(4)	
F1				
x	0.0897(4)	0.0872(5)	0.0865(4)	0.0877(3)
y	0.4722(4)	0.4741(5)	0.4716(4)	0.4730(3)
z	¼	¼	¼	¼
B (Å^2)	1.17(5)	0.80(9)	0.71(6)	
F2				
x	0.7028(3)	0.7030(3)	0.7031(3)	0.7025(2)
y	0.2964(3)	0.2953(3)	0.2953(3)	0.2949(2)
z	0.0476(2)	0.0464(3)	0.0468(2)	0.0459(1)
B (Å^2)	1.20(4)	0.92(8)	0.80(5)	

[a] Synthesized in air; agreement factors: $R_p = 10.7\%$, $R_{wp} = 14.0\%$, $R_F = 3.7\%$, $\chi^2 = 1.63$
[b] Synthesized in air; agreement factors: $R_p = 3.0\%$, $R_{wp} = 4.0\%$, $R_F = 3.6\%$, $\chi^2 = 3.35$
[c] Displacement factors refined anisotropically

exceed 3% of the strongest perovskite line, i.e., $(200)_{Pm\bar{3}m}$. In both cases, the appearance of Mg compounds in the sample probably results from minor loss of alkalis owing to reaction of NaF and KF with the crucible walls. Several XRD patterns of the end-member neighborite prepared in air and nitrogen flow under different heating regimes ($T = 750$–800 °C, $\tau = 5$–10 h) were refined independently, and found to produce virtually identical results. Excellent correspondence was also observed among intermediate members of the neighborite series prepared under different synthesis conditions (see figures and tables below). In our opinion, this indicates that the loss of alkalis (or decomposition) during the experiment was minimal and did not affect phase relationships in the series investigated.

End-member perovskites

End-member $NaMgF_3$ ($x = 0$) is structurally very well characterized (Zhao et al. 1993a, b, 1994; Rönnebro et al. 2000). This compound is isostructural with orthorhombic $GdFeO_3$-type perovskites (*Pbnm*, $a \approx \sqrt{2}a_p$, $b \approx \sqrt{2}a_p$, $c \approx \sqrt{2}a_p$, $Z = 4$). The results of profile refinement of XRD and ND patterns of neighborite are in good agreement with the previously published structural data

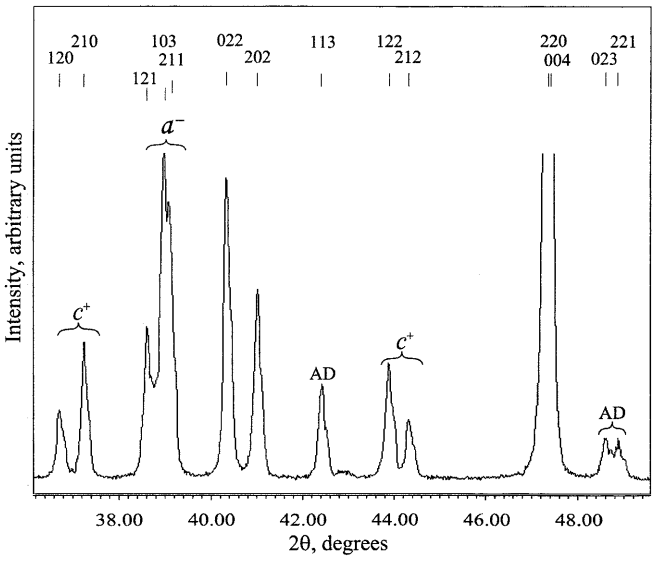

Fig. 1 Representative fragment of the measured XRD pattern of $NaMgF_3$ (Cu$K\alpha$ radiation) showing superlattice reflections indicative of antiphase tilting (a^-) and in-phase tilting (c^+) of MgF_6 polyhedra, and *A*-site cation displacement (*AD*)

(Table 2). The diffraction patterns of $NaMgF_3$ are characterized by the presence of strong superlattice reflections indicative of rotation (tilting) of the MgF_6 octahedra in the structure (Fig. 1). Diffraction lines with l even and either h or k odd in the *Pbnm* setting (e.g., the doublet $\{120 + 210\}_{Pbnm}$) arise from an in-phase tilting about the c axis of the pseudocubic subcell. Lines with l odd and either h or k even (e.g., $\{121 + 103 + 211\}_{Pbnm}$) indicate antiphase rotations of the octahedra about the a and b axes. Finally, peaks with l odd, and both h and k either even or odd arise from antiparallel displacements of Na^{1+} cations within the mirror planes, i.e., perpendicular to $[001]_{Pbnm}$ (Zhao et al. 1993b).

The potassium end member ($x = 1.00$) has an undistorted cubic structure (space group $Pm\bar{3}m$) characteristic of the perovskite aristotype (e.g., Burns et al. 1996). In this structure, the Mg, K, and F atoms occupy the 1*a*, 1*b*, and 3*d* sites, respectively. The XRD and ND patterns of $KMgF_3$ lack superstructure reflections indicative of octahedral rotation or cationic displacements. The unit-cell parameters determined for the cubic end member in this study [$a = 3.9897(1)$ Å from XRD, and $a = 3.9908(3)$ Å from ND data] are notably higher than the parameter $a = 3.9859(8)$ Å reported by Burns et al. (1996). This discrepancy may result from the fact that Burns et al. (1996) obtained their value using the cell-refinement program of Appleman and Evans (1973) rather than by full-profile refinement.

Intermediate members

Careful examination of XRD powder patterns shows that in the series $(Na_{1-x}K_x)MgF_3$, three major changes occur with increasing potassium content (x):

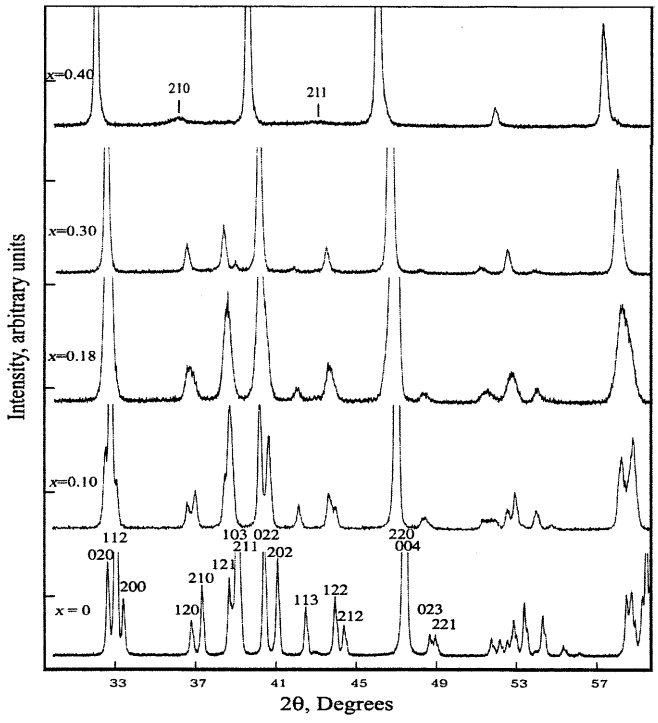

Fig. 2 Evolution of position and intensity of superlattice peaks on the measured XRD patterns of neighborite $(Na_{1-x}K_x)MgF_3$ in the compositional range $0 \le x \le 0.40$ (Cu$K\alpha$ radiation). The superlattice peaks are indexed selectively on an orthorhombic *Pbnm*-type cell ($x = 0$) and a tetragonal *P4/mbm*-type cell ($x = 0.40$)

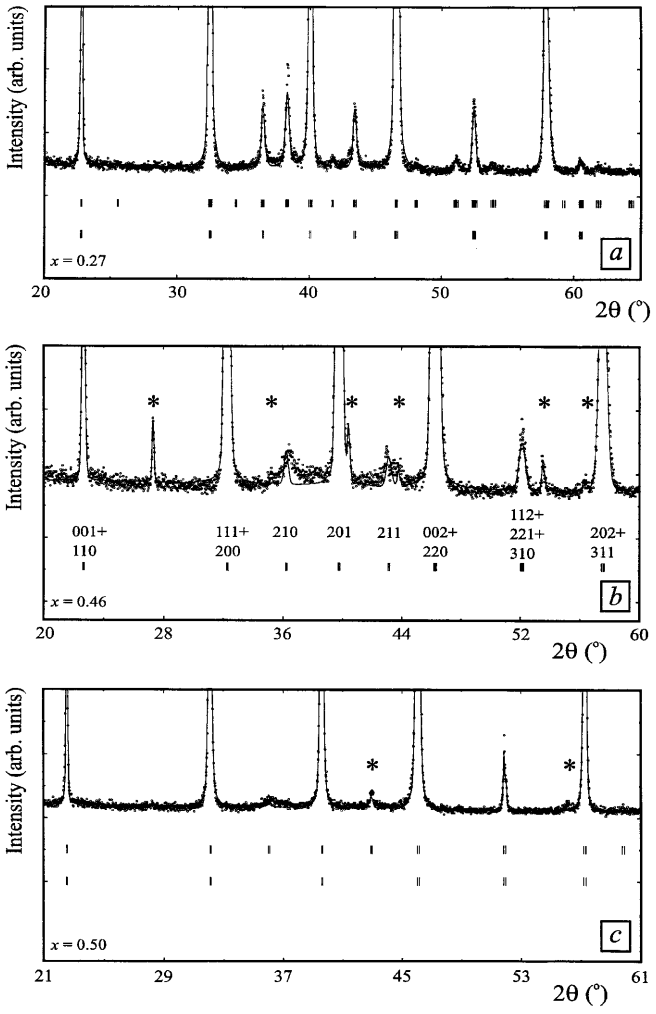

Fig. 3a–c Selected XRD patterns of orthorhomic (**a**), tetragonal (**b**), and cubic (**c**) neighborite compositions approaching the inferred phase-transition points. *Dots* correspond to the measured, and *lines* to the calculated patterns (Cu$K\alpha$ radiation). **a** Calculated peak positions are given for the *Pbnm* (*upper row*) and *P4/mbm* models. **b** Peak positions and indices only for the tetragonal model are given. **c** Calculated peak positions for both *P4/mbm* (*upper row*) and $Pm\bar{3}m$ models are indicated. Peaks corresponding to impurity phases (MgF_2 and MgO) are denoted by *asterisks* (*)

1. Diffraction lines with odd-odd-odd and even-even-odd indices reduce in intensity and disappear in the compositional range $0.30 < x < 0.40$. This feature reflects a decrease in the magnitude of *A*-cation displacement in the $(001)_{Pbnm}$ plane.

2. Diffraction lines with even-odd-odd and odd-even-odd indices reduce in intensity and disappear in the compositional range $0.30 < x < 0.40$, whereas lines with *l* even and either *h* or *k* odd coalesce at $x = 0.40$ to form a single reflection (Fig. 2). These changes clearly demonstrate that the antiphase tilt component is not present in neighborite with over 40 mol% $KMgF_3$ (cf. Fig. 3a, b). The superlattice reflections indicative of in-phase tilting of the MgF_6 octahedra persist through the compositional range $0.40 \le x \le 0.46$.

3. Reflections produced by coalescence of odd-even-even and even-odd-even peaks (*Pbnm* setting) vanish at K concentrations above $x = 0.50$. There is neither antiphase nor in-phase octahedral rotation present in the K-dominant members of the neighborite series.

The above-described features indicate that the orthorhombic $GdFeO_3$-type structure is stable in the compositional range $0 \le x < 0.40$. The refinement results for a representative sample of orthorhombic neighborite with a moderate K content are given in Table 3. The disappearance of "antiphase" and "displacement" superlattice reflections at $x = 0.40$ indicates a phase transition to a perovskite structure with only the in-phase tilt component present. The superlattice diffraction lines with two indices odd and one even indicate a tetragonal structure derived from the perovskite aristotype by in-phase octahedral tilting, i.e., a *P4/mbm*-type cell with $a \approx \sqrt{2}a_p$, $c \approx a_p$ and $Z = 2$ (Ahtee and Darlington 1980). A noteworthy feature of the diffraction patterns in the tetragonal structural range and for the most K-rich orthorhombic compounds ($x \ge 0.27$) is broadening of the superlattice reflections, which probably results from the presence of domains in the sample. Individual domains may be associated with antiphase boundaries (short-range order between the *A*-site cations) or variation in structural distortion over the sample (e.g., orthorhombic enclaves in a tetragonal matrix). The existence of domains in the series

$(Na_{1-x}K_x)MgF_3$ was confirmed by the preliminary TEM examination of samples $x = 0.40$ and 0.50 by one of the authors (R.H.M.).

The superlattice reflections are virtually indistinguishable on the diffraction patterns of $(Na_{0.5}K_{0.5})MgF_3$ (Fig. 3c). Refinement of these patterns on the basis of the tetragonal and cubic structural models gives comparable results (Table 4). The XRD pattern of $x = 0.56$ is best refined assuming the undistorted cubic structure. We also attempted to refine the diffraction patterns of $x = 0.50$ and 0.56 as a mixture of two perovskite phases with different symmetry, but the refinement results were unsatisfactory in both cases. Hence, the disappearance of the lines characteristic of in-phase octahedral tilting at $x \approx 0.50$ indicates a further phase transition to the undistorted cubic structure. This structural type persists over a wide range of neighborite compositions with more than 50 mol% $KMgF_3$.

The results of the present study are summarized in Table 5 and Figs. 4 to 8. Table 5 and Fig. 4 demonstrate that introduction of K^{1+} into the structure of neighborite results in a dramatic increase in the unit-cell parameters: on average, by about 0.016 Å per 10 mol% $KMgF_3$. The cell expansion clearly results from a larger ionic radius of K^{1+} in comparison with Na^{1+} (1.64 and 1.39 Å, respectively: Shannon 1976). As a total expansion of the perovskite subcell over the complete range of compositions is 0.16 Å, the estimated difference in radii between K^{1+} and Na^{1+} is $\sqrt{2} \times 0.16 = 0.23$ Å. This value is in excellent agree-

Table 3 $(Na_{1-x}K_x)MgF_3$: crystallographic characteristics, selected interatomic distances and bond angles for $x = 0.18$ (XRD data). Final agreement factors and cell parameters (*Pbnm*): $R = 12.5\%$, $R_{wp} = 16.6\%$, $R_F = 4.8\%$, $\chi^2 = 1.78$, $a = 5.4486(5)$, $b = 5.5101(5)$, $c = 7.7623(8)$ Å

Atom	Position	x	y	z	B (Å^2)
A[a]	4*c*	0.9911(8)	0.0244(6)	¼	2.09(5)
Mg	4*b*	½	0	0	0.94(4)
F1	4*c*	0.0778(9)	0.4831(8)	¼	1.4(1)
F2	8*d*	0.7084(5)	0.2876(5)	0.0290 (5)	1.62(8)

AF_9 polyhedron:		MgF_6 polyhedron:	
A-F1	2.360 Å	2 × Mg-F1	1.988 Å
A-F1	2.571 Å	2 × Mg-F2	1.962 Å
A-F1	3.020 Å	2 × Mg-F2	1.986 Å
2 × *A*-F2	2.414 Å	2 × Mg-F1-Mg	154.8°
2 × *A*-F2	2.677 Å	2 × Mg-F2-Mg	157.8°
2 × *A*-F2	2.724 Å		

[a] A = Na, K

Table 4 $(Na_{1-x}K_x)MgF_3$ ($x = 0.5$): refinement results (ND data) for two alternative structural models

	Tetragonal model	Cubic model		Tetragonal model	Cubic model
Space group	*P*4/*mbm*	*Pm*$\bar{3}$*m*	R_p	4.8%	4.8%
a(Å)	5.566(3)	3.9354(1)	R_{wp}	6.3%	6.4%
c(Å)	3.953(4)		R_F	2.8%	2.1%
a_p(Å)	3.942(3)		χ^2	2.47	2.54
A[a]			F1		
x	0	½	*x*	0	½
y	½	½	*y*	0	0
z	½	½	*z*	½	0
B (Å^2)	1.1(1)	1.0(1)	*B* (Å^2)	1.97 (8)	2.05 (8)
Mg			F2		
x	0	0	*x*	0.2596 (10)	
y	0	0	*y*	0.7596 (10)	
z	0	0	*z*	0	
B (Å^2)	−0.5 (1)	−0.6 (1)	*B* (Å^2)	1.96 (8)	

[a] A = Na, K

Table 5 $(Na_{1-x}K_x)MgF_3$: unit-cell parameters (Å), refined positions of oxygen atoms, tilt angles (°) and polyhedral volumes (Å^3). All compounds in *plain font* synthesized in air, those *in italic* synthesized in nitrogen flow

x	a	b	c	ϕ	θ	Φ	V_A (V_A, actual)$_{CN^a}$	V_B	V_A/V_B
Orthorhombic (*Pbnm*)									
0	5.3607(1)	5.4873(8)	7.6662(1)	10.6	14.9	18.2	45.98 (24.76)$_{VIII}$	10.40	4.42
0	*5.3613(1)*	*5.4867(1)*	*7.6668(1)*	*10.5*	*14.9*	*18.1*	*46.00 (24.77)$_{VIII}$*	*10.39*	*4.42*
0.09	5.4101(2)	5.4985(2)	7.7160(3)	9.4	13.2	16.1	47.02 (32.25)$_{IX}$	10.36	4.54
0.10	*5.4097(2)*	*5.4981(2)*	*7.7151(3)*	*9.4*	*14.1*	*16.9*	*47.02 (32.24)$_{IX}$*	*10.36*	*4.54*
0.18	5.4486(5)	5.5101(5)	7.7623(8)	9.0	11.0	14.2	47.94 (32.81)$_{IX}$	10.32	4.65
0.27	5.4954(3)	5.5209(3)	7.8069(4)	7.9	8.0	11.2	48.96 (40.05)$_{X}$	10.25	4.78
0.30	5.5054(5)	5.5263(3)	7.8179(5)	7.3	6.7	10.0	49.26	10.20	4.83
Tetragonal (*P4/mbm*)									
0.40	5.5459(3)		3.9232(3)	4.8			51.05	10.13	5.04
0.46	5.5464(6)		3.9303(8)	4.5			51.11	10.14	5.04
Cubic (*Pm*$\bar{3}$*m*)									
0.50	3.9403(1)						50.98	10.20	5.00
0.56	3.9492(1)						51.32	10.26	5.00
0.60	*3.9545(1)*						*51.53*	*10.31*	*5.00*
0.67	3.9622(1)						51.84	10.37	5.00
0.70	*3.9659(2)*						*51.98*	*10.40*	*5.00*
0.78	3.9742(1)						52.31	10.46	5.00
0.89	3.9824(1)						52.63	10.53	5.00
1.00	3.9897(1)						52.92	10.58	5.00

[a] Given only for neighborite with A-site cations coordinated by fewer than 12 atoms of fluorine; the actual coordination number is denoted by subscript

ment with the difference of 0.25 Å derived from the data of Shannon (1976). This observation further supports our conclusion that there was no significant loss of alkalis from the experimental charges during the sample preparation.

Figure 5 shows variation in fractional atomic displacements (as defined by Zhao et al. 1993b) with composition. The displacement values gradually diminish towards the phase transition at $x \approx 0.40$, and only the parameters u_{F2} and v_{F2} continue into the tetragonal structural range. The actual value of atomic displacement along $(001)_{Pbnm}$ calculated from u_A and v_A decreases from ca. 0.25 Å at $x = 0$ to zero above $x = 0.30$. Note that shift of F atoms from the special positions can be used to calculate a degree of distortion of the hettotype (derivative) structure. The structure of end-member neighborite is derived from the aristotype by a combination of two antiphase and one in-phase rotations of the MgF_6 octahedra about the fourfold axes of the cubic subcell, i.e., $a^-a^-c^+$ according to the Glazer (1972) classification of tilted octahedra in perovskites. For simplicity, this composite octahedral rotation can be split into tilt θ about $[110]_{Pm3m}$ and tilt ϕ about $[001]_{Pm\bar{3}m}$ (Zhao et al. 1993b). For orthorhombic perovskites, a vector combination of θ and ϕ can be expressed as single rotation Φ about a threefold axis of the cubic subcell (O'Keeffe and Hyde 1977). The three tilts can be estimated from fractional atomic displacements or unit-cell parameters (Zhao et al. 1993b). Values calculated from the atomic coordinates of F are relatively insensitive to distortions of the MgF_6 polyhedra, and thus more accurately reflect deviation of the crystal structure from the $Pm\bar{3}m$ parent. Figure 6 demonstrates how the θ, ϕ, and Φ tilts vary with composition. The tilt angles derived by two different methods are in reasonable agreement with each other, and show a gradual decrease throughout the orthorhombic structural range. As indicated by the disappearance of superlattice reflections with even-odd-odd and odd-even-odd indices, only the in-phase tilt component (ϕ) persists into the tetragonal range. This type of distortion corresponds to the tilt system $a^0a^0c^+$ in Glazer's notation (1972). The ϕ tilt is further eliminated by a transition to the undistorted cubic structure above $x = 0.46$. In agreement with the experimental results of Zhao (1998), our data indicate that a transition from

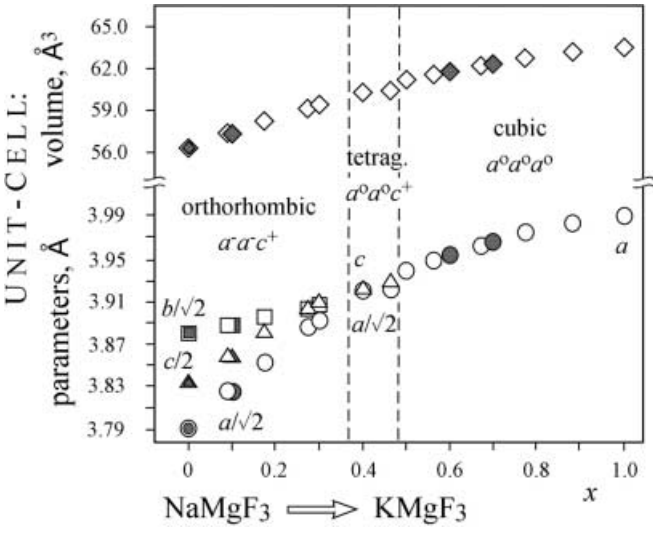

Fig. 4 Variation of unit-cell parameters and volumes (reduced to pseudocubic for low-symmetry compounds) throughout the neighborite series $(Na_{1-x}K_x)MgF_3$. *Empty symbols* correspond to compounds synthesized in air, and *shaded symbols* to those synthesized in an N_2 flow

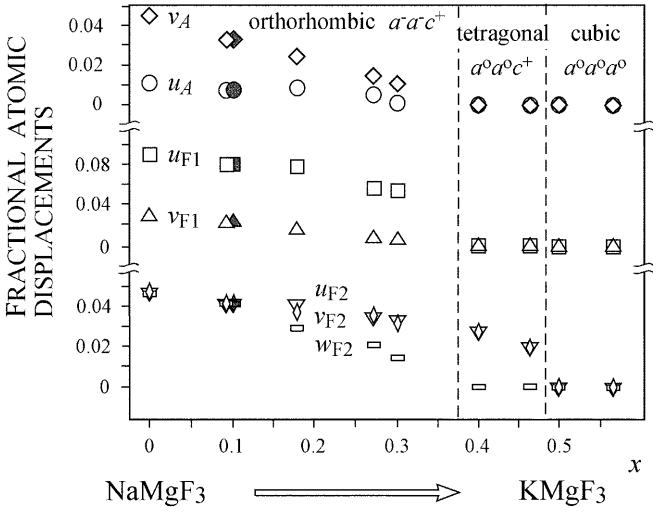

Fig. 5 Variation in fractional atomic coordinates (for definition see Zhao et al. 1993b) throughout the compositional range $0 \le x \le 0.56$. *Empty symbols* correspond to $(Na_{1-x}K_x)MgF_3$ compounds synthesized in air, and *shaded symbols* to those synthesized in an N_2 flow

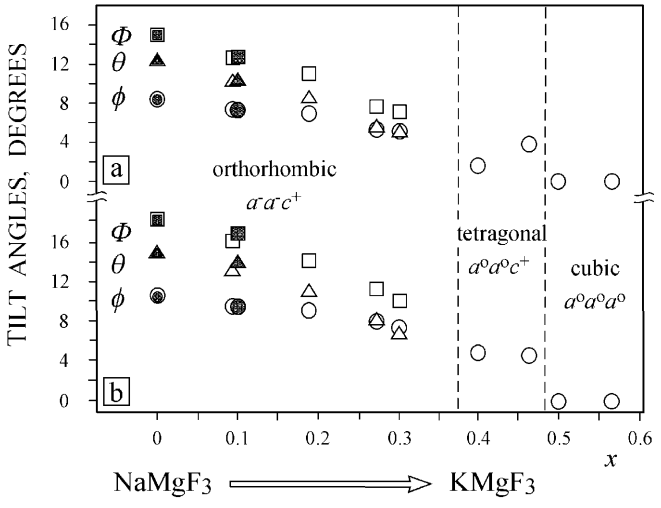

Fig. 6a–b Variation of tilt angles calculated from unit-cell parameters (**a**) and fractional atomic coordinates (**b**) throughout the compositional range $0 \le x \le 0.56$. *Empty symbols* correspond to $(Na_{1-x}K_x)MgF_3$ compounds synthesized in air, and *shaded symbols* to those synthesized in an N_2 flow

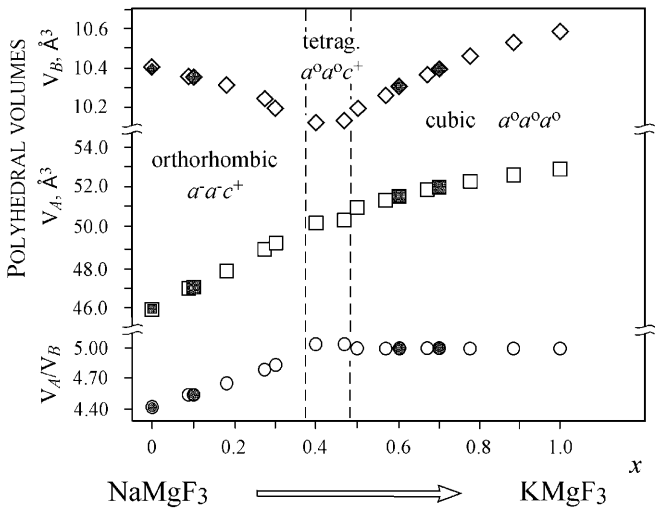

Fig. 7 Variation of polyhedral volumes and polyhedral-volume ratio throughout the neighborite series $(Na_{1-x}K_x)MgF_3$. *Empty symbols* correspond to compounds synthesized in air, and *shaded symbols* to those synthesized in an N_2 flow

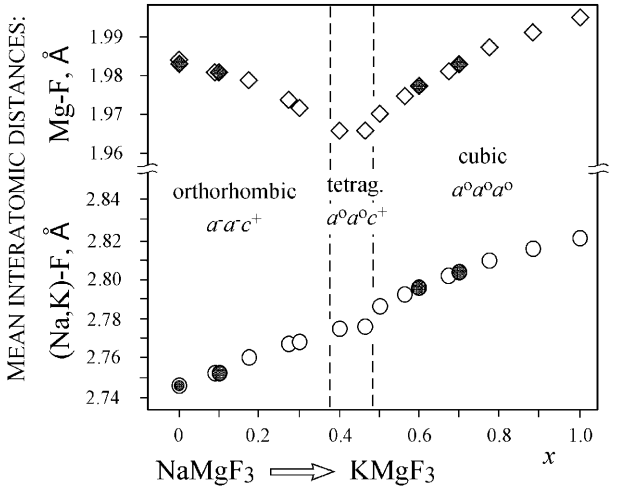

Fig. 8 Variation of mean cation–anion distances throughout the neighborite series $(Na_{1-x}K_x)MgF_3$. *Empty symbols* correspond to compounds synthesized in air, and *shaded symbols* to those synthesized in an N_2 flow

the three-tilt orthorhombic structure ($a^-a^-c^+$) to one-tilt tetragonal ($a^0a^0c^+$) is direct, and does not involve formation of an intermediate two-tilt perovskite near the transition point.

Alternatively, the degree of structural distortion can be expressed via the ratio between volumes of $(Na,K)F_{12}$ and MgF_6 polyhedra (Thomas 1996). From geometric considerations, the polyhedral volume ratio in undistorted cubic perovskites is 5.00. As octahedral tilting normally leads to a decrease in the volume of the central 12-coordinated polyhedron, the ratio V_A/V_B decreases progressively with deviation of the structure from ideal cubic. Although the effective coordination number of the *A*-site cation in orthorhombic neighborite is 8, 9, or 10 (Table 3), the polyhedral volume must be calculated for a 12-coordinated polyhedron to allow comparison with the data for the tetragonal and cubic perovskites: $V_A = (V_{cell}/Z) - V_B$ (Thomas 1996). As expected, the polyhedral volume ratio increases with x approaching 5.00 at the boundary between the tetragonal and cubic structural regions (Fig. 7). It has been suggested that *Pbnm*-type structures are most stable at $V_A/V_B < 4.7$, although the polyhedral volume ratios cited for orthorhombic perovskites in the literature range from 4.1 to 4.9 (Thomas 1998). The end-member $NaMgF_3$ shows a steady increase in V_A/V_B towards a temperature-induced transition to the cubic symmetry, from 4.4 at 25 °C to 5.0 at the transition point (Thomas 1998).

The substitution of Na^{1+} by comparatively larger K^{1+} leads to increasing mean interatomic distances between the *A*-site cations and fluorine (Fig. 8). Interestingly, the mean Mg–F distance demonstrates a drastically different behavior, i.e., it first decreases with x and, above $x = 0.40$, rapidly increases towards the potassium end member. A broadly similar variation pattern was observed for the series $(Na_{1-x}K_x)MgF_3$ by Zhao (1998: Fig. 6). However, his results indicate a nearly constant Mg–F bond length of ca. 1.98 Å, and the maximum compression of the MgF_6 polyhedra at $x = 0.35$. According to Zhao et al. (1993a) and Zhao (1998), the observed shortening of the Mg–F bond is associated with a decrease in octahedral tilting near the phase transition, and parallels critical softening phenomena near the temperature-induced $Pbnm \Rightarrow Pm\bar{3}m$ transition in pure $NaMgF_3$.

Discussion and conclusions

The general sequence of phase transitions observed in the present study is in agreement with that determined by Zhao (1998), i.e., $Pbnm \Rightarrow P4/mbm \Rightarrow Pm\bar{3}m$, with increasing K contents. In his study, Zhao (1998) postulated that the orthorhombic phase coexists with the tetragonal phase in the compositional range $0.15 \le x < 0.30$. In our series of experiments, we observed no indication of such sample heterogeneity (e.g., overlapping reflections or anomalous behavior of unit-cell parameters). Further, according to Zhao (1998), the agreement factors R_p, R_{wp}, and χ^2 significantly improve when the tetragonal phase is introduced into the refinement. To test this possibility, we rerefined several selected XRD patterns on the basis of the two-phase structural model. As suggested by Zhao (1998), the two-phase refinements do converge with somewhat improved R_p, R_{wp}, and χ^2 factors. However, the two-phase refinements invariably yield higher isotropic thermal parameters of F atoms in comparison with the one-phase refinements incorporating only the *Pbnm* phase. For most of the compounds, the *B* parameters of F atoms in the *P4/mbm* component exceed 3.7 Å^2, and thus are considered unsatisfactory. Note that in Zhao's refinements (1998: Table 1), the isotropic thermal parameters

were fixed at the same values for both perovskite phases. Furthermore, according to this author, the relative proportion of the tetragonal component is maximal (ca. 45% of the sample) at approximately $x = 0.15$, which results in anomalous behavior of the tilt angles and mean interatomic distances close to that composition (Zhao 1998: Figs. 5, 6, and 16). Therefore, we find no conclusive evidence for the coexistence of two structurally different perovskite phases in our samples. We also suggest that "fitting" of composite two-phase peaks into the observed diffraction lines may not be a valid procedure for two topologically and dimensionally similar structures, although such an approach does produce statistically "improved" results. Finally, we believe that cocrystallization of orthorhombic and tetragonal perovskites with *identical* compositions over a range of ~30 mol% $KMgF_3$ is implausible because of the very large difference in ionic radii between K^{1+} and Na^{1+}. If the presence of the two structurally distinct perovskites were confirmed by independent methods, occupancy of the *A* site by K^{1+} and Na^{1+} would have to be refined to determine whether the two phases are true polymorphs or simply compositions that delineate a miscibility gap.

There is also minor disagreement between the data of Zhao (1998) and those obtained in the present work as to the relative position of the phase transitions along x. Zhao (1998, p. 124) suggests that "the perovskite structure becomes purely tetragonal *P4/mbm*" at $x = 0.35$. However, the XRD pattern of this compound obtained in the present work contains weak superlattice reflections indicative of the antiphase octahedral tilting. Also, the two components of the doublet $\{122 + 212\}_{Pbnm}$ are well resolved, and do not form a single $(211)_{P4/mbm}$ line as on the patterns of tetragonal neighborite. As we discussed above, the pattern of $x = 0.56$ is devoid of superlattice reflections, and best refined as cubic. Thus, we infer that the $Pbnm \Rightarrow P4/mbm$ and $P4/mbm \Rightarrow Pm\bar{3}m$ phase transitions occur at ca. 40 and 50 mol% $KMgF_3$, respectively.

One of the most interesting conclusions with regard to the crystal chemistry of fluoride perovskites in the system $(Na_{1-x}K_x)MgF_3$ is that long-range cation ordering is not present in this solid solution, and K^{1+} and Na^{1+} cations are distributed over the *A* sites at random. However, we expect that the 19% difference in ionic radius should have some effect on the distribution of the univalent cations, and suggest that the broadening of superlattice reflections observed for the intermediate compounds may reflect short-range order between the *A*-site cations. A detailed transmission-electron microscopy study of neighborite in the compositional range $0.3 \le x \le 0.5$ is required to identify the true nature of domains.

Acknowledgements This work was supported by the Natural Sciences and Engineering Research Council of Canada and Lakehead University, Ontario (Canada). Two anonymous reviewers are thanked for their constructive comments on the earlier version of this paper. We are also grateful to Dr. Anatoly Zaitsev for his comments on the occurrence of neighborite at Khibina.

References

Ahtee M, Darlington CNW (1980) Structures of sodium tantalate (V) by neutron powder diffraction. Acta Crystallogr (B) 36: 1007–1014

Appleman DE, Evans HT (1973) Job 9214: indexing and least-squares refinement of powder diffraction data. US Geol Surv Comput Contrib 20 NTIS Doc PB 2–16 188

Arkhangel'skaya VV (1974) Neighborite from Eastern Siberia. Doklady AN SSSR Earth Sci Sect 210: 131–134

Burns PC, Hawthorne FC, Hofmeister AM, Moret SL (1996) A structural phase transition in $K(Mg_{1-x}Cu_x)F_3$ perovskite. Phys Chem Miner 23: 141–150

Chao ECT, Evans HT, Skinner BJ, Milton C (1961) Neighborite, $NaMgF_3$, a new mineral from the Green River Formation, South Ouray, Utah. Am Mineral 46: 379–393

Flocken JW, Smith RW, Hardy JR, Stevenson ES, Swearingen J (1996) Phase transitions in mixed alkali calcium trifluoride solid solutions. Mater Res Bull 31: 1093–1099

Glazer AM (1972) The classification of tilted octahedra in perovskites. Acta Crystallogr (B) 28: 3384–3392

Horváth L, Gault RA (1990) The mineralogy of Mont Saint-Hilaire, Quebec. Mineral Rec 21: 281–359

Jouanneaux A, Daniel Ph, Bushnell-Wye G (1998) Structural instabilities in disordered perovskites $Rb_{1-x}K_xCaF_3$ studied by synchrotron radiation powder diffraction. Proposition for a phase diagram. J Phys Condens Matter 10: 5485–5502

Mitchell RH (1997) Carbonate-carbonate immiscibility, neighborite and potassium iron sulphide in Oldoinyo Lengai natrocarbonatite. Mineral Mag 61: 779–789

Mo Z, Flocken JW, Mei WN (1990) The crossover of phase transitions from $NaCaF_3$ to $KCaF_3$. Ferroelectr 120: 157–165

O'Keeffe M, Hyde BG (1977) Some structures topologically related to cubic perovskite ($E2_1$), ReO_3 ($D0_9$) and Cu_3Au ($L1_2$). Acta Crystallogr (B) 33: 3802–3813

Raade G, Haug J (1980) Rare fluorides from a soda granite in the Oslo region, Norway. Mineral Rec 11: 83–91

Rodriguez-Carvajal J (1990) "FULLPROF" program: Rietveld pattern matching analysis of powder patterns. ILL, Grenoble, France

Rönnebro E, Noreus D, Kadir K, Reiser A, Bogdanovic B (2000) Investigation of the perovskite-related structures of $NaMgH_3$, $NaMgF_3$ and Na_3AlH_6. J Alloys Comp 299: 101–106

Shannon RD (1976) Revised effective ionic radii and systematic studies of interatomic distances in halides and chalcogenides. Acta Crystallogr (A) 32: 751–767

Thomas NW (1996) The compositional dependence of octahedral tilting in orthorhombic and tetragonal perovskites. Acta Crystallogr (B) 52: 16–31

Thomas NW (1998) A new global parametrization of perovskite structures. Acta Crystallogr (B) 54: 585–599

Yefimov AF, Yes'kova YM, Katayeva ZT (1967) The first discovery of neighborite in the USSR. Doklady AN SSSR Earth Sci Sect 174: 140–142

Zaitsev AN (1992) The mineralogy of carbonatites of the Khibina massif, and their major genetic features (in Russian). Unpubl PhD Thesis, St Petersburg State University

Zhao Yu (1998) Crystal chemistry and phase transitions of perovskite in *P-T-X* space: data for $(K_xNa_{1-x})MgF_3$ perovskites. J Solid State Chem 141: 121–132

Zhao Yu, Weidner DJ, Parise JB, Cox DE (1993a) Thermal expansion and structural distortion of perovskite – data for $NaMgF_3$ perovskite. Part I. Phys Earth Planet Int 76: 1–16

Zhao Yu, Weidner DJ, Parise JB, Cox DE (1993b) Critical phenomena and phase transition of perovskite – data for $NaMgF_3$ perovskite. Part II. Phys Earth Planet Int 76: 17–34

Zhao Yu, Parise JB, Wang Ya, Kusaba K, Vaughan MT, Weidner DJ, Kikegawa T, Chen J, Shimomura O (1994) High-pressure crystal chemistry of neighborite, $NaMgF_3$: an angle-dispersive diffraction study using monochromatic synchrotron X-radiation. Am Mineral 79: 615–621